J. Fluid Mech. (1983), *vol.* 126, *pp.* 507–520
Printed in Great Britain

The breaking and non-breaking wave resistance of a two-dimensional hydrofoil

By JAMES H. DUNCAN
Hydronautics Incorporated, 7210 Pindell School Road, Laurel, Maryland 20707

(Received 19 February 1982 and in revised form 2 July 1982)

Measurements of the surface-height profile and the vertical distributions of velocity and total head were made behind a two-dimensional fully submerged hydrofoil moving horizontally at constant speed and angle of attack. These measurements were used to resolve the drag on the foil into two parts: one associated with the turbulent breaking region that is sometimes present on the forward face of the first wave, and the other associated with the remaining non-breaking wavetrain. It was found that at 'incipient breaking' the first wave existed in either a breaking or a non-breaking state depending on the starting procedures. It was possible to induce steady breaking when the wave slope was 17° or higher. The wake survey measurements showed that the drag associated with breaking reached more than three times the maximum drag that could theoretically be obtained with non-breaking waves. The drag associated with breaking was found to be proportional to the downslope component of the weight of the breaking region.

1. Introduction

The wave resistance of a body moving near the free surface of a fluid can be dissected into two parts: one associated with the non-breaking waves that are radiated away from the body and the other associated with the wave energy that is dissipated by breaking. This situation was first described by Froude (1955), '...the ship in its passage along the surface of the water has to be continually supplying the waste of an attendant system of waves, which, from the nature of their constitution as independent waves are continually diffusing or transmitting themselves into the surrounding water or, where they form what is called broken water, crumbling away into froth'. Our quantitative understanding of non-breaking wave resistance has been greatly improved since the time of Froude. On the other hand breaking resistance received little attention until Baba (1969) showed that as much as 15% of the resistance of a full-form ship was associated with its breaking bow wave. Other experimental studies and observations of ship-generated breaking waves have been reported by Taneda (1974), Kayo & Takekuma (1981), Baba (1976), Miyata, Inui & Kajitani (1980) and Miyata (1980). Reviews of ship-wave phenomena including some discussion of wave breaking have been given by Wehausen (1973), Tulin (1978) and Inui (1981).

Duncan (1981) has performed an extensive experimental study of breaking waves produced by a fully submerged, two-dimensional hydrofoil in steady horizontal motion. A schematic of the flow is shown in figure 1. The results of this study support the hypothesis that the turbulent breaking region of the wave imparts a shearing force along the forward slope equal to the component of its weight in that direction. The force produces a turbulent, momentum-deficient wake at the water surface (see

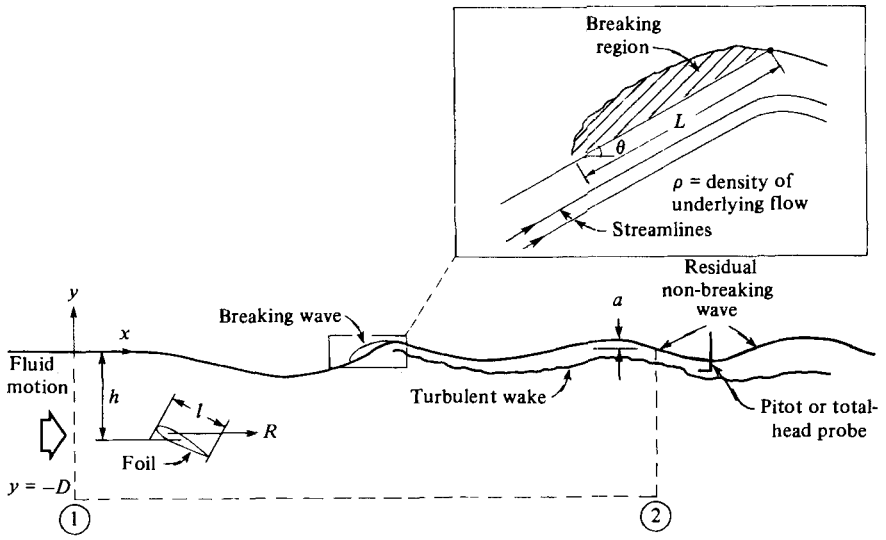

FIGURE 1. Schematic of breaking wave and following wavetrain.

figure 1). Battjes & Sakai (1981) have made turbulence measurements in the wake of a similar hydrofoil-produced breaker. However, they reported no correlations between these measurements and geometrical properties of the breaking wave.

The present paper describes further experiments with hydrofoil-produced breaking waves. The objective of this new set of measurements is to resolve the wave resistance of the foil into its non-breaking-wave and breaking-wave components, to examine the breaking criterion, and to relate the geometry of the breaking region to the breaking-wave drag. Section 2 describes the details of the experimental apparatus and measurement techniques. This is followed in §3 by a presentation of the experimental results, which are later discussed in §4. Finally the conclusions of the work are summarized in §5.

2. Experimental details

2.1. *Apparatus*

The hydrofoil was towed in a tank that was 24 m long, 61 cm deep, and 61 cm wide (see figure 2). One of the 24 m long sidewalls of the tank was made of clear Plexiglas, while the other three walls and the bottom were plywood. For photography, the bottom and the 24 m long plywood wall were covered with black cloth. There were $\pm 0{\cdot}5$ cm variations in the depth and width of the tank.

The hydrofoil had a NACA 0012 shape and was made of solid aluminium. It had a chord of 20·3 cm and a maximum thickness of 2·54 cm at 6·1 cm from the nose. The span of the foil was only 60·0 cm to ensure clearance along the entire tank. There was initial concern that the gaps between the foil edges and the walls, which varied from 2 to 5 mm, might cause unwanted three-dimensional effects. Wave measurements, however, showed no discernible lack of two-dimensionality. The foil was towed along a pair of 20 m long aluminium tracks – one attached to each side of the tank at a nominal distance of 15 cm from the tank bottom. When the installation of the rails was complete, measurements showed that the depth of the rails from the water surface did not vary by more than 0·2 cm at any point in the tank. The foil was attached to the rails through two thin nylon blocks, which were

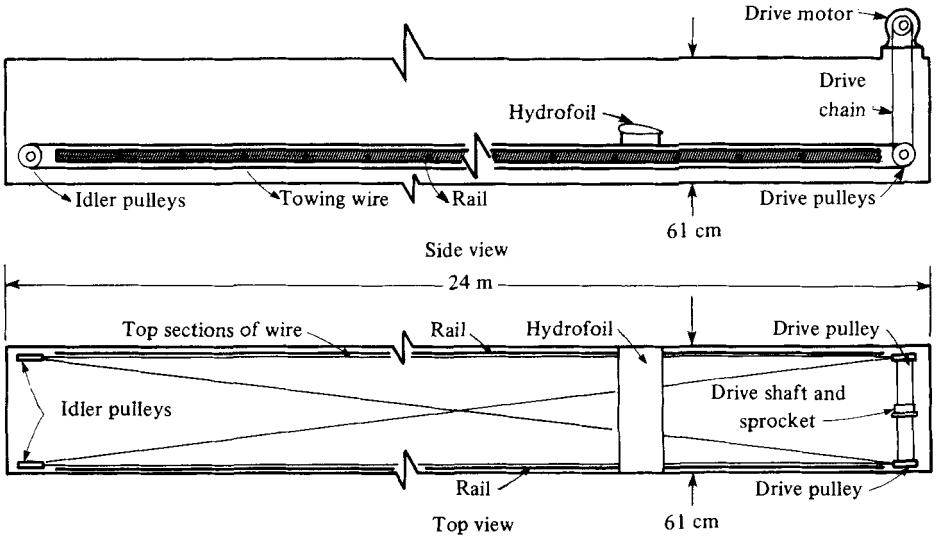

FIGURE 2. Towing tank with foil and its towing system.

bolted to the bottom of the foil on either side. The foil could be set at either a 5° or 10° angle of attack, nose up.

The force for moving the foil through the water was supplied by a wire-and-pulley towing system (see figure 2). The power for the towing system came from an electric motor and a variable-speed transmission, which were mounted on top of the tank. A roller chain and sprocket transmitted power from the motor to the pulley drive shaft. To prevent roller-chain grease from producing a surface slick on the water, a barrier was placed at the surface next to the chain. The foil could be towed at speeds up to 1·2 m/s; and nothing pierced the water surface in the vicinity of the foil. Reproducibility checks on the speed, which were made by timing the foil over 13 m, showed only a 1 % fluctuation in speed at 1·2 m/s.

2.2. *Measurements*

The measurements included height profiles of non-breaking waves, geometrical characteristics of the breaking region, and vertical distributions of the velocity and total head in the wake of the breaker (see figure 1). The non-breaking wave profiles were measured with a capacitance wave height guage utilizing a Teflon-coated, 0·020 in. diameter wire. The response of the probe was checked and found to be more than adequate for measuring the steep ($ak \approx 0{\cdot}31$) low-frequency (≈ 2 Hz) waves considered here.

The geometry of the breaking region was measured using a 16 mm ciné camera attached to an independently controlled carriage that travelled on top of the tank. The camera was mounted on the carriage by a wood frame, which placed it at a horizontal distance of 1·1 m from the Plexiglas side wall and at various heights. Along with the camera, the carriage contained a light-slit generator consisting of five 500 W photofloodlights and two vertical metal plates. This device could project a 3 cm thick vertical sheet of light, 1·2 m long, parallel to the long sidewalls of the tank along the tank's centre. The camera was placed about 15 cm above the water surface and 1·1 m out from the tank sidewall, oriented to point slightly down toward the water surface. The water was dyed with 1·5 p.p.m. rhodamine-WT fluorescent dye. When the

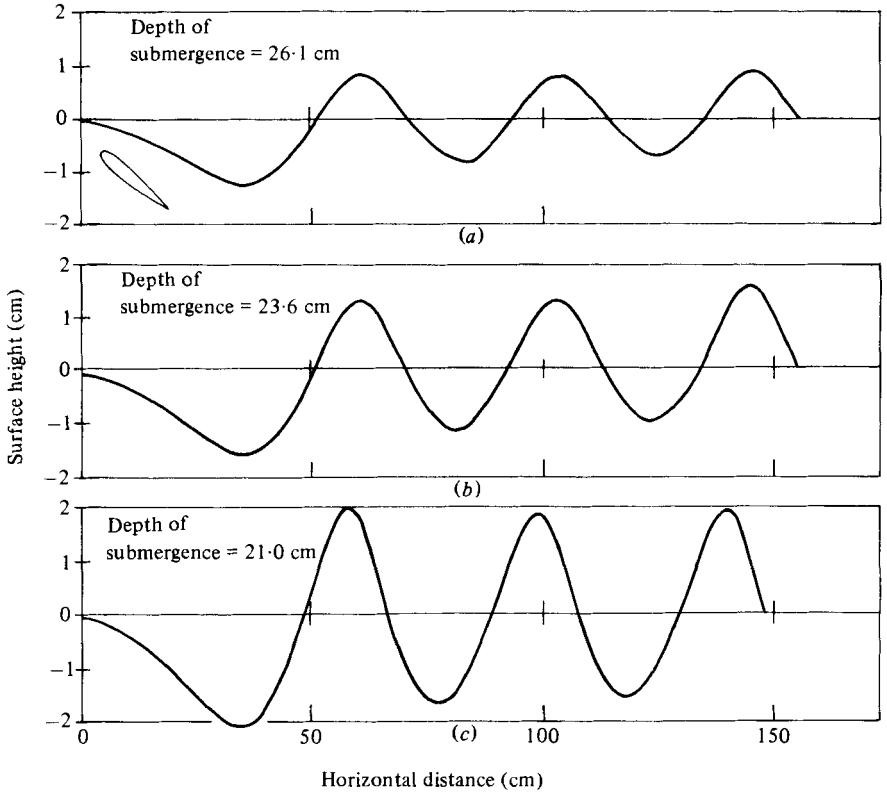

FIGURE 3 (*a–c*). For caption see facing page.

lights were on, fluorescence of the dye was excited only within the vertical sheet of light. The camera then recorded a glowing line on the water surface, which, when the wave was present, produced an image of the surface profile at the centre of the tank. Distances were measured to an accuracy of about $\pm 0{\cdot}3$ cm. The average values of the variables describing the breaking region were obtained from films taken in wave-fixed coordinates. The first measurement was always taken when the foil was at least 6 m from the starting position to ensure a quasi-steady state.

The velocity and total head distributions were measured using 0·16 mm diameter Pitot and total-head tubes connected to a Pace diaphragm-type pressure transducer. The probes were mounted on the upper carriage. The starting characteristics of the two motors driving the foil and the carriage were such that the probe could be positioned behind the foil during an experimental run to an accuracy of plus or minus 1·0 cm in the horizontal. The resulting signal was filtered to remove noise from the carriage vibration and then recorded on a strip chart recorder. The average value during the run was then read from the chart.

3. Results

3.1. *Breaking criteria*

The breaking criteria was explored through a series of experiments with foil speeds of 60·0 and 100 cm/s at a 5° foil angle of attack, and with 80 cm/s at angles of attack of 5° and 10°. For each of the four combinations of speed and angle of attack a set of runs was performed with various total water depths. During all runs the foil was

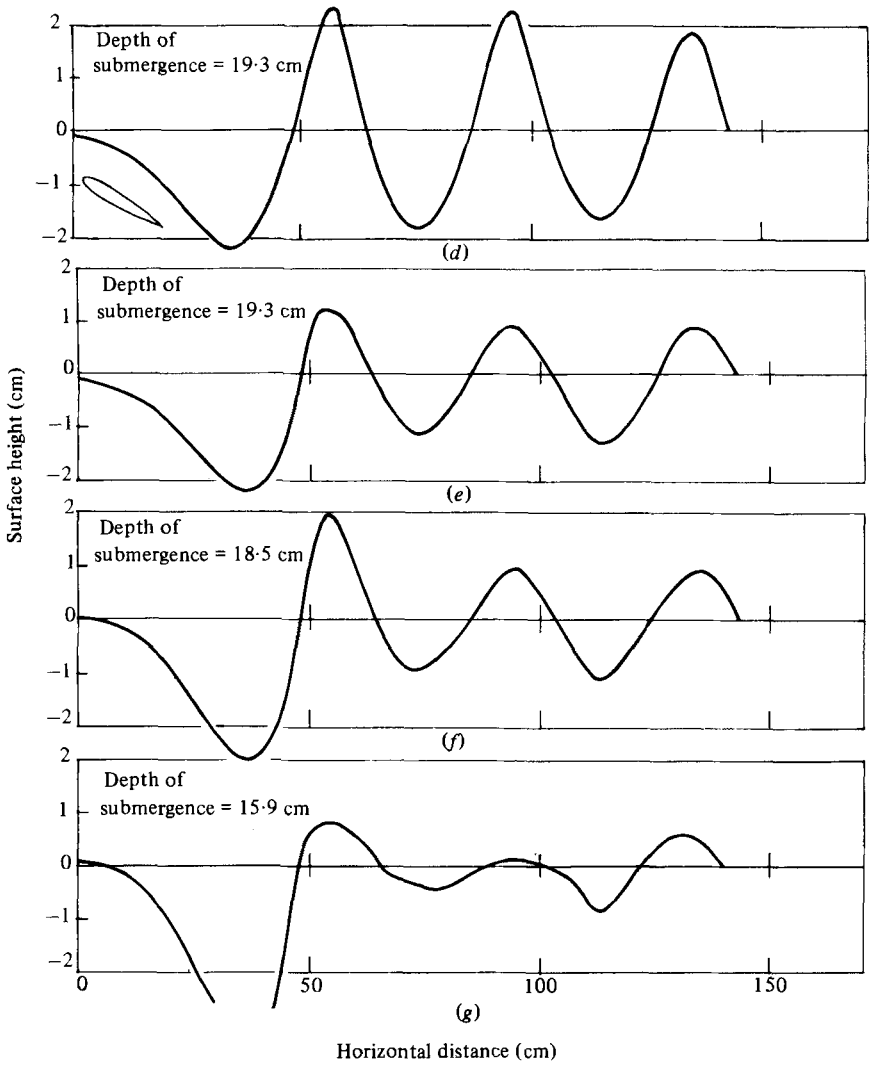

FIGURE 3. Wave profiles for foil speed = 80 cm/s, angle of attack = 5°, various depths of submergence.

at a fixed height, 17·5 cm above the tank bottom. Thus by lowering the water level the depth of submergence of the foil could be decreased. Since the chord of the foil was 20·3 cm, the flow field around the foil was certainly influenced by the floor of the tank. The length of the waves produced, however, was never more than 1·4 times the total water depth; thus the wave dynamics were not significantly influenced by the bottom. In an infinitely deep tank the depth of submergence of the foil at incipient breaking would be different than it was here since the lift on the foil would change if the bottom were removed. The wave slope at that point, however, would probably be the same as in the present case. With the above considerations in mind, changes in total water level will be referred to as changes in depth of submergence hereinafter.

Several of the profiles measured at 80 cm/s and 5° angle of attack are shown in figure 3. The uppermost profile is for the largest depth of submergence and contains only small-amplitude, non-breaking waves. As the depth was decreased, the steepness of the wavetrain increased. When the depth was small enough the first wave in the

train began to break. As the depth was decreased further the breaking became more intense and the steepness of the residual wavetrain following the breaker decreased. Similar sets of profiles were taken at the other foil speeds and angles of attack.

The transition from a non-breaking to a breaking wave occurred over a range of submergence depths of about 0·5 cm. Inside this range it was possible to induce steady breaking by disturbing the, otherwise, non-breaking wavetrain. Let us denote the greatest and smallest depths in this range by d_i and d_s respectively. For depths greater than d_i, disturbing the non-breaking wavetrain did not result in a steady breaking wave. For depths less than d_s, wave breaking occurred spontaneously. The profiles shown in figures 3(*d*, *e*) are for the same depth of submergence in the range between d_i and d_s. The profile of the wavetrain in the breaking state is shown in figure 3(*e*), while the corresponding non-breaking profile is shown in figure 3(*d*). The disturbance used to start the breaking process was a surface current created by dragging a light cloth on the water surface. The cloth was placed ahead of the foil and pulled at the foil speed for a few seconds as the foil started from rest. The cloth was then removed and the breaking process continued unaided for the remainder of the run.

The influence of surface currents on incipient breaking conditions was first recognized by Banner & Phillips (1974). Their idea was basically a modification of the Stokes (1847) zero-surface-current breaking criterion. Stokes showed that in a wave of maximum slope (incipient breaking) the fluid velocity at the crest is equal to the wave phase speed. In the presence of a surface current in the direction of the wave travel, this condition can be met at a smaller wave slope. Thus in the present experiments, the cloth-induced surface current initiated breaking in waves of small slope. When the wave slope was steep enough, breaking continued after the cloth was removed.

Profiles of the non-breaking waves at depths d_i and d_s were measured and analysed for each of the four combinations of foil speed and angle of attack. The wave profiles measured at d_s showed no common characteristics. For instance, the maximum inclination of the wave face from the horizontal varied from 16° to 24°. Similar results were found by Salvesen (1981). The data taken from the wave profiles measured at d_i is shown in table 1. The average of the angle of inclination data is $17° \pm 1°$. A slight increase in the angle with increasing speed can be seen, but this is within the $\pm 1°$ accuracy of the measurement. The crest-to-trough height divided by the wavelength (H/L) has an average of 0·1. Note that these values are considerably less than the theoretical values (30° and $H/L = 0{\cdot}14$) calculated by Schwartz (1974) and others.

3.2. *Wave resistance*

Three measurements are necessary to determine the resistance of the foil due to breaking and non-breaking waves. These are the vertical distributions of velocity and of total head defect and the surface height at some point behind the foil. The total head defect is the difference between the total head at the measuring point and the total head upstream of the body. A derivation of the equation used for the resistance evaluation from these measurements is given in §4.2. Typical distributions of total head defect and horizontal velocity at the second trough behind the breaker are shown in figures 4 and 5 respectively. The total head defect was, of course, zero in the region below the turbulent wake of the breaker, and reached a maximum at the water surface. If the data were taken at even greater depths the defect due to the turbulent wake of the foil would appear in the data. However, the wake of the foil was not of interest in the present study and was ignored. The velocity profile also shows the

Foil speed (cm/s)	Foil angle of attack	Wavelength λ (cm)	Crest-to-trough amplitude $2a$ (cm)	$\frac{2a}{\lambda}$	Inclination of forward face measured from horizontal	Average inclination
60·0	5°	23·1	2·5	0·108	14·8°	15·5° ± 1·0°
60·0	5°	23·1	2·5	0·108	16·2°	
80·1	5°	41·8	4·0	0·095	15·8°	17·1° ± 1·2°
80·1	5°	41·8	4·2	0·100	18·0°	
80·1	5°	41·8	4·2	0·100	17·6°	
80·1	10°	41·7	4·4	0·105	17·6°	17·4° ± 0·4°
80·1	10°	41·7	4·4	0·105	17·1°	
100·2	5°	60·1	5·9	0·099	18·2°	18·0° ± 0·4°
100·2	5°	61·2	6·2	0·101	18·2°	
100·2	5°	61·2	6·0	0·098	17·5°	

TABLE 1. Wave-profile data at upper stability boundary; average $2a/\lambda = 0{\cdot}102 \pm 0{\cdot}004$, average inclination = $17{\cdot}1° \pm 1{\cdot}2°$

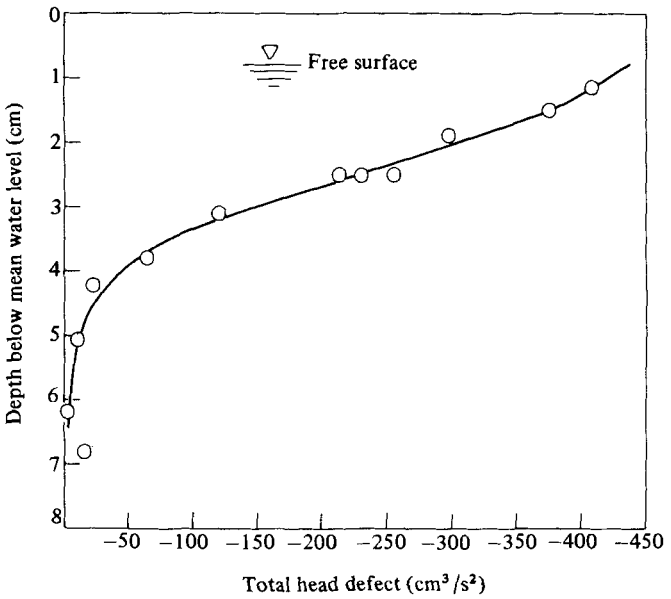

FIGURE 4. Total head defect versus depth; foil speed = 80 cm/s, angle of attack = 5°, depth of submergence = 18·5 cm, second trough after the breaker.

wake of the breaker at the surface. Below the surface wake the measured distribution follows the theoretical distribution of velocity for a linear Stokes wave with the same speed and amplitude as the residual wavetrain following the breaker. Inside the surface wake, the velocity is seen to be lower than the Stokes-wave calculation. As the depth of submergence decreased, the maximum total head defect increased and the surface velocity decreased. The above measurements were used to compute the wave drag on the hydrofoil, and the results are presented and discussed in §4.

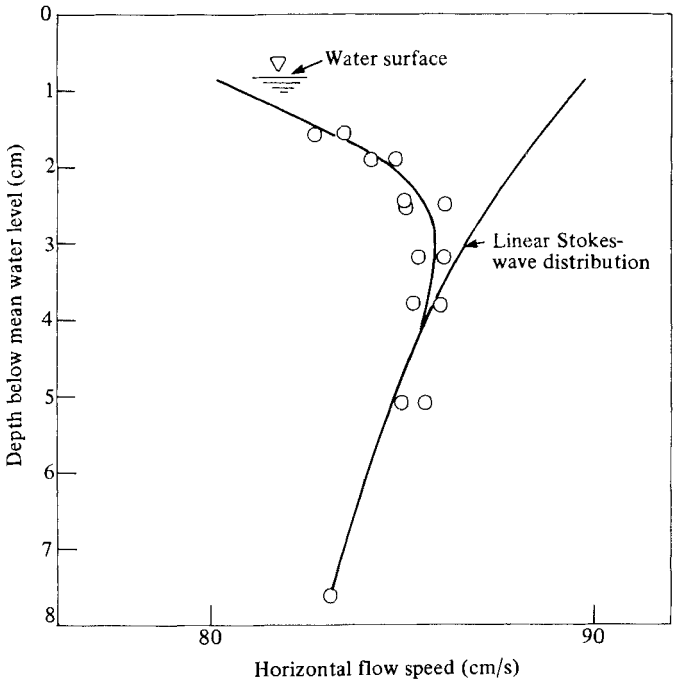

FIGURE 5. Horizontal flow velocity versus depth; foil speed = 80 cm/s, angle of attack = 5°, depth of submergence = 18·5 cm, second trough after the breaker.

3.3. *Breaking-region geometry*

Measurements of the area of the breaking region and the angle of inclination of the forward face of the wave (see figure 1) were taken for a foil speed of 80 cm/s, an angle of attack of 5°, and four depths of submergence. In order to relate these measurements to the breaking-wave resistance three of these conditions were chosen to correspond to cases where the drag was determined from flow measurements. The area of the breaking region and the angle of inclination of the forward face of the wave are plotted versus depth of submergence in figure 6. Note that as the depth decreased the area increased while the angle of inclination decreased. An extensive set of measurements of this type can be found in Duncan (1981).

4. Discussion

4.1. *Breaking criteria*

The transition from the steady non-breaking wave to the steady breaking wave displays characteristics common to many stability phenomena. The stability parameter in this case is the slope of the wave. As the depth of submergence is decreased, the slope increases. At shallow slopes no disturbance can induce a steady breaking wave. Once the slope is 17° (when the depth of submergence reaches d_i) a large disturbance (the surface current) can cause the otherwise laminar flow to change to an alternative steady breaking flow. At slopes larger than 17° a transition to the breaking state occurs spontaneously. It is believed that small flow perturbations (starting transients) cause the transition to the breaking state at this point. These starting transients were not controlled in the present experiments. It is believed that they were responsible for the scatter in the wave-slope data measured at the depth of submergence d_s. The dynamics of these transients are explained below.

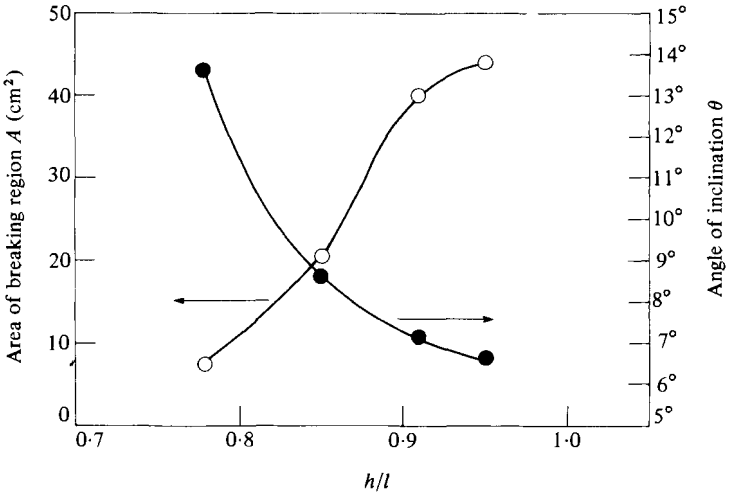

FIGURE 6. Area of breaking region and angle of inclination of the wave face versus dimensionless depth of submergence (See figure 1 for definitions).

When the foil starts from rest it produces a spectrum of waves. The shape of this spectrum is controlled by the acceleration history, angle of attack, final speed, and depth of submergence of the foil. Of the transient waves the one with the most potential to influence the final steady wavetrain is the one whose group velocity equals the final foil speed. This wave travels with the foil; all others either move ahead or are left behind. On the other hand the steady wave pattern travels with phase velocity equal to the foil speed. Let k_s and C_s denote the wavenumber and phase velocity of the steady wavetrain. Let k_t and C_{gt} denote the wavenumber and group velocity of the transient wave component whose group velocity equals the steady foil speed. Then by linear theory

$$C_{gt} = \frac{1}{2}\left(\frac{g}{k_t}\right)^{\frac{1}{2}} = \left(\frac{g}{k_s}\right)^{\frac{1}{2}} = C_s. \tag{1}$$

Thus we have

$$k_s = 4k_t. \tag{2}$$

From (2) we see that the length of the transient wave is four times the length of the steady wave. The stability of an infinite wavetrain with subharmonic disturbances of this type was explored theoretically by Longuet-Higgins (1978). Figure 6 of that paper shows that for a basic wavetrain steepness of about $ak_s = 0{\cdot}314$ (the approximate slope at d_s) the fastest-growing subharmonic is the one with four times the basic wavelength. Though the wavetrain in the present experiments is not infinite we may conjecture that this result applies generally in the present case. Thus it seems that incipient spontaneous breaking is induced by unstable subharmonic disturbances produced as the foil starts from rest. At the induced breaking boundary these disturbances are probably too small or their growth rates too low to induce breaking in the available time of travel of the foil.

4.2. *Resistance*

The resistance associated with both breaking and non-breaking waves was determined from measurements of the surface height and the vertical distributions of velocity and total head defect at the second trough behind the breaking wave. The formula for the resistance is derived below. Let us begin by writing the spatially integrated horizontal momentum equation and the continuity equation for the control volume

enclosed by the dashed line in figure 1:

$$\frac{R}{\rho} = \int_{-D}^{\eta_1} \left(\frac{P_1}{\rho} + C^2\right) dy - \int_{-D}^{\eta_2} \left(\frac{P_2}{\rho} + u_2^2\right) dy + \int_{x_1}^{x_2} uv\Big|_{y=-D} dx, \tag{3}$$

$$\int_{-D}^{\eta_1} C\, dy = \int_{-D}^{\eta_2} u_2\, dy - \int_{x_1}^{x_2} v\, dy, \tag{4}$$

where R is the total wave resistance of the foil per unit length (the wake of the foil is ignored in this analysis), x and y are the horizontal and vertical coordinates, u and v are the corresponding velocity components, P is the pressure and ρ is the density. The bottom of the control volume is at $y = -D$, and subscripts 1 and 2 refer to the upstream and downstream ends of the control volume. The line $y = 0$ is chosen so that the average surface height far downstream of the breaker is zero, while the surface height upstream is taken as η_1 to allow for the possibility of a mean-water-level change.

As the depth $-D$ becomes large, the last integral in (3) can be approximated by $c_1 \int v\, dx$, which can then be eliminated by use of (4). Thus we have

$$\frac{R}{\rho} = -\int_{-D}^{\eta_2} \left(\frac{P_2}{\rho} + u_2^2\right) dy + \int_{-D}^{\eta_1} \frac{P_1}{\rho} dy - C \int_{-D}^{\eta_2} u_2\, dy. \tag{5}$$

Since the pressure is hydrostatic at station 1, the upstream pressure term in (5) may be transformed as follows:

$$\int_{-D}^{\eta_1} \frac{P_1}{\rho} dy = \int_{-D}^{\eta_2} \frac{P_1}{\rho} dy + \tfrac{1}{2} g(\eta_2^2 - \eta_1^2). \tag{6}$$

Now defining the total head functions

$$G_1 = \frac{P_1}{\rho} + \tfrac{1}{2}(u_1^2 + v_1^2) + gy, \tag{7a}$$

$$G_2 = \frac{P_2}{\rho} + \tfrac{1}{2}(u_2^2 + v_2^2) + gy, \tag{7b}$$

and using these to eliminate the pressures, we have

$$\frac{R}{\rho} = \int_{-D}^{\eta_2} \{G_1 - G_2 + \tfrac{1}{2}v_2^2 - \tfrac{1}{2}(u_2 + C)^2\}\, dy + \tfrac{1}{2} g(\eta_2^2 - \eta_1^2). \tag{8}$$

Equation (8) is the equation for the resistance including the drag associated with both breaking and non-breaking waves. This result reduces to the result of Duncan (1981) when the slope of the residual wavetrain is small.

In the case where there is no wave breaking, $G_1 = G_2$ everywhere in the flow and (8) takes the same form as that given by Wehausen & Laitone (1960). In this case the velocities can be found in terms of the surface height using potential-flow wave theory. This analysis was performed by Duncan (1982) utilizing third-order Stokes-wave theory and the finite-amplitude numerical results of Longuet-Higgins (1975). It was shown that the maximum non-breaking-wave resistance, $R_{\max}$ on a two-dimensional body moving at speed C, is $0{\cdot}02\rho C^4/g$. This provides an important numerical value for comparison with the drag associated with breaking.

The drag results are shown in figure 7. These are plots of dimensionless resistance R^* versus dimensionless depth of submergence for foil speeds 60, 80 and 100 cm/s respectively. The angle of attack was 5° in all cases. The depth was non-dimensionalized

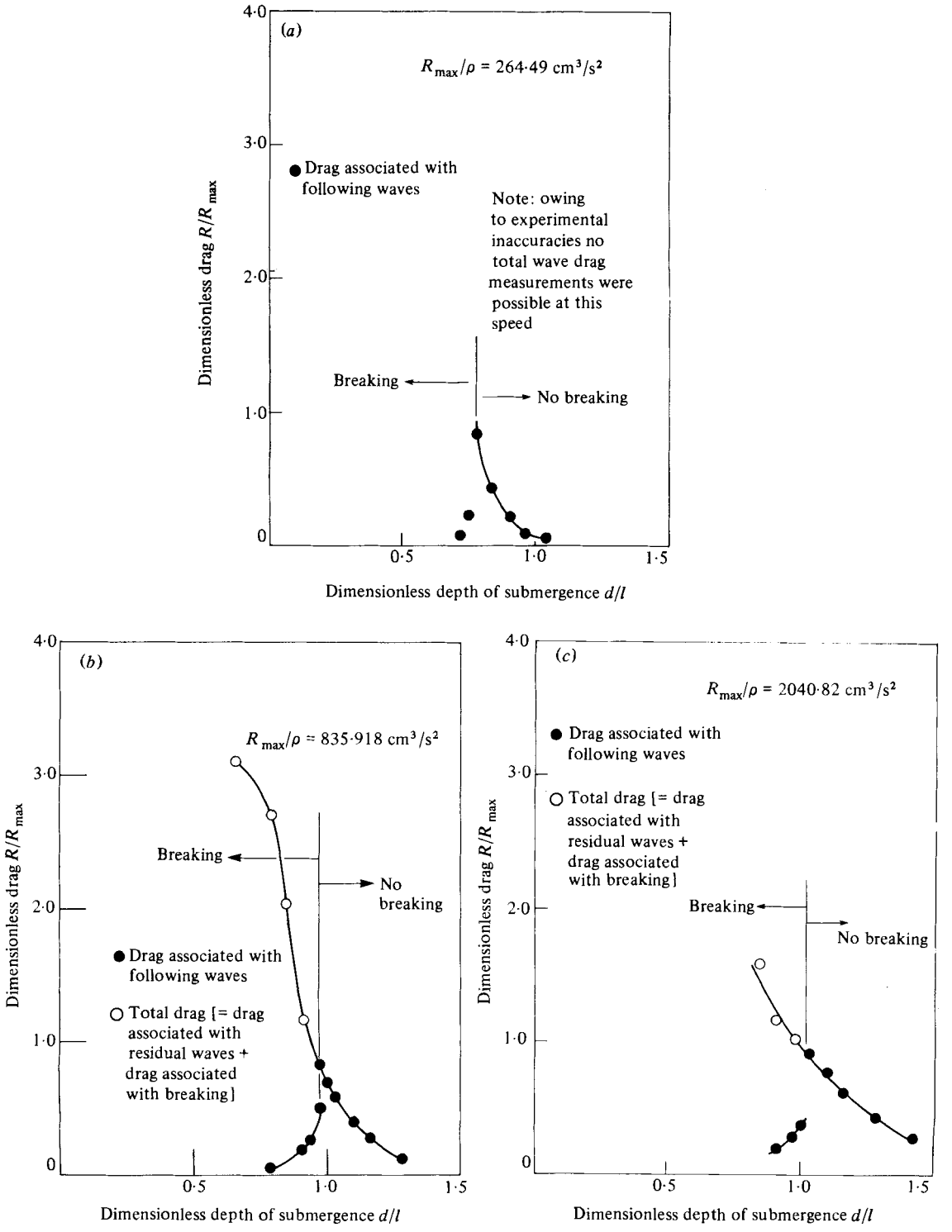

FIGURE 7. Wave drag versus depth of submergence; angle of attack = 5° and foil speed: (*a*) 60 cm/s, (*b*) 80 cm/s, (*c*) 100 cm/s.

by the chord of the foil while the drag was non-dimensionalized by $R_{\max}$ – the theoretical maximum non-breaking drag. The figures show two types of points. The black circles were obtained by using the average amplitude of the residual non-breaking wavetrain in the potential-flow results of Duncan (1982). Thus they represent the drag associated with the residual wavetrain. The open circles represent evaluations of (8) using the flow measurements. These points include the resistance associated with both the breaking wave and the residual wavetrain. The drag associated with breaking is thus the total wave drag (open circles) minus the residual wave drag (black circles).

The three resistance plots all show a similar behaviour. At large depths the waves were of small amplitude and no breaking occurred. The drag, determined from wave-height measurements, was a small fraction of the maximum potential-flow resistance. As the depth was decreased, the non-breaking resistance increased rapidly. The largest resistance measured without breaking was 0·83 in all cases. When the depth was further decreased, breaking began and the drag associated with the residual wavetrain decreased rapidly. At the same time the total drag increased even more rapidly, reaching 3·1 times the maximum potential-flow drag $0{\cdot}02\rho C^4/g$. At this point the drag associated with the residual wavetrain was nearly zero.

There are three distinct flow regimes in each of these resistance plots. For dimensionless resistances R^* ($= Rg/0{\cdot}02\rho c^4$) between 0 and 0·83 the flow exists only in the non-breaking state; the waves are not steep enough to support a steady breaking zone. For R^* between 0·83 and 1·0 two flow states can exist (one breaking and one non-breaking) that can produce the same resistance on the foil. Both states were found in the experiments when R^* was near 0·83, but only the breaking state was found for R^* near 1·0. Presumably the non-breaking state could be realized experimentally throughout this regime if flow disturbances could be avoided (see §4.1). For R^* greater than 1·0 the flow exists only in the turbulent breaking state; it is not theoretically possible to have a non-breaking flow state with a resistance this high.

4.3. *Breaker geometry*

The production of the surface wake and the simultaneous suppression of the residual wavetrain is brought about by the turbulent breaking region riding the forward slope of the first wave behind the foil (see figure 1). Duncan (1981) has shown that the momentum deficit in the wake is proportional to $\rho g A \sin\theta$, the component of the breaking region's weight that is tangent to the wave face. To complete the present data set a plot of $\rho g A \sin\theta$ versus the breaking resistance is given in figure 8. The figure includes data from Duncan (1981) and data from the present study. The systematic differences between the two data sets is probably due to the difficulties involved in estimating the streamline separating the breaking region from the underlying flow (see Duncan 1981). However, both sets show a straight-line behaviour, and the average slope of the line is 1·9.

5. Conclusion

The present experimental investigation has shown that there are three distinct flow regimes associated with the wave system behind a towed hydrofoil (see figure 8). When the total dimensionless wave resistance R^* (the total wave resistance divided by the maximum theoretical non-breaking resistance) is between 0 and 0·83 only non-breaking waves appear behind the foil. For $0{\cdot}83 \leqslant R^* \leqslant 1{\cdot}0$ it is possible for either

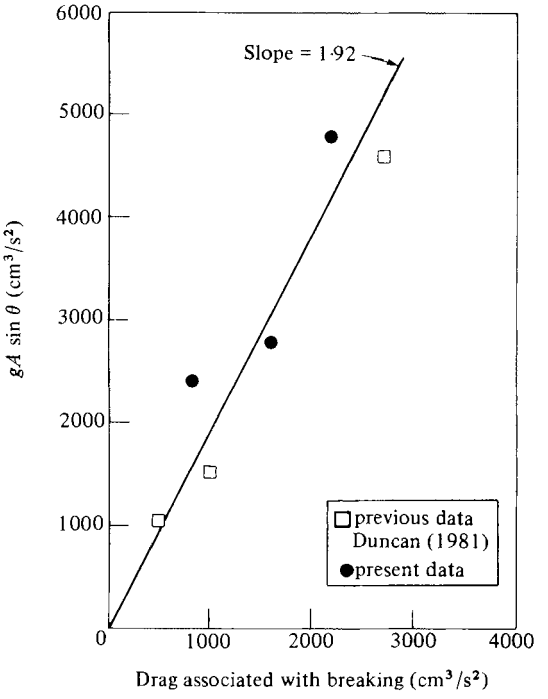

FIGURE 8. Tangential component of the breaking region's weight versus drag associated with breaking.

a breaking or a non-breaking flow state to exist: each can have the same total wave resistance ($R^* = 0{\cdot}83$ corresponds to a wave slope of 17°). Both states are found in the experiments when R^* is near 0·83, but only the breaking state is found for R^* near 1·0. Presumably the non-breaking state could also be realized experimentally for R^* near 1·0 if disturbances could be avoided (see §4.1). In this regime when the flow is in the breaking state the residual wavetrain resistance is about equal to the breaking resistance. For R^* greater than 1·0 the flow exists only in the turbulent breaking state experimentally. It is not theoretically possible to have a non-breaking flow state with a resistance this large. In the cases with the most vigorous breaking, R^* values as high as 3·1 are found; here the resistance due to the residual wavetrain is negligible.

This work was supported by the Naval Sea Systems Command General Hydromechanics Research Program administered by the David Taylor Naval Ship Research and Development Center under contract N00014-80-C-0118.

REFERENCES

BABA, E. 1969 A new component of viscous resistance. *J. Soc. Nav. Arch. Japan* **125**, 23.

BABA, E. 1976 Wave breaking resistance of ships. In *Proc. Int. Seminar on Wave Resistance, Tokyo*, pp. 75–92.

BANNER, M. L. & PHILLIPS, O. M. 1974 On the incipient breaking of small scale waves. *J. Fluid Mech.* **65**, 647–656.

BATTJES, J. A. & SAKAI, T. 1981 Velocity field in a steady breaker. *J. Fluid Mech.* **111**, 421–437.

DUNCAN, J. H. 1981 An experimental investigation of breaking waves produced by a towed hydrofoil. *Proc. R. Soc. Lond.* A **377**, 331–348.

DUNCAN, J. H. 1982 A note on the evaluation of the wave resistance of two-dimensional bodies from measurements of the downstream wave profile. *J. Ship Res.* (in the press).

FROUDE, W. 1955 *The Papers of William Froude.* London: The Institution of Naval Architects.

INUI, T. 1981 From bulbous bow to free-surface shock wave – trends of 20 years' research on ship waves at the Tokyo University tank. *J. Ship Res.* **25**, 147–180.

KAYO, Y. & TAKEKUMA, K. 1981 On the free-surface shear flow related to bow wave-breaking of full ship models. *J. Soc. Nav. Arch. Japan* **149**, 11–20.

LONGUET-HIGGINS, M. S. 1975 The integral properties of periodic gravity waves of finite amplitude. *Proc. R. Soc. Lond.* A **342**, 157–174.

LONGUET-HIGGINS, M. S. 1978 The instabilities of gravity waves of finite amplitude in deep water. II. Subharmonics. *Proc. R. Soc. Lond.* A **360**, 489–505.

MIYATA, H. 1980 Characteristics of nonlinear waves in the near-field of ships and their effects on resistance. In *Proc. 13th Symp. on Naval Hydrodynamics, Tokyo*, pp. III-5-1–III-5-17.

MIYATA, H., INUI, T. & KAJITANI, H. 1980 Free surface shock waves around ships and their effects on ship resistance. *Nav. Arch. & Ocean Engng, Soc. Nav. Arch. Japan* **18**, 1–9.

SALVESEN, N. 1981 Five years of numerical naval ship hydrodynamics at DTNSRDC. *J. Ship Res.* **25**, 219–235.

SCHWARTZ, L. W. 1974 Computer extension and analytic continuation of Stokes' expansion for gravity waves. *J. Fluid Mech.* **62**, 553–578.

STOKES, G. G. 1847 On the theory of oscillatory waves. *Trans. Camb. Phil. Soc.* **8**, 441.

TANEDA, S. 1974 Necklace vortices. *J. Phys. Soc. Japan* **36**, pp. 298–303.

TULIN, M. P. 1978 Ship wave resistance – a survey. In *Proc. 8th U.S. Nat. Congr. Applied Mech., Los Angeles.*

WEHAUSEN, J. 1973 The wave resistance of ships. *Adv. Appl. Mech.* **13**, 93–245.

WEHAUSEN, J. & LAITONE, E. V. 1960 Surface waves. In *Handbuch der Physik*, vol. 9. Springer.